Hindawi
Advances in Materials Science and Engineering
Volume 2023, Article ID 8051118, 18 pages
https://doi.org/10.1155/2023/8051118

Research Article

The Optimization of the Fillet Size of Autoclave Tooth Based on the Experiment and Numerical Simulation

Xiaoping Ouyang, Zhijian Ye, Pengcheng Lin, and Yanping Li

Guangdong Institute of Special Equipment Inspection and Research Huizhou Branch, Guangdong, China

Correspondence should be addressed to Zhijian Ye; yzj2008080808@163.com

Received 16 December 2022; Revised 8 March 2023; Accepted 11 March 2023; Published 8 May 2023

Academic Editor: Mehran Khan

Focusing on the phenomenon of the crack on the autoclave flange, a three-dimensional model of the autoclave was established based on the Ansys Workbench platform. A new finite element analysis flow for optimizing the design of autoclave teeth was established using the Fluent, Static Structure, and Direct Optimization modules. The paper analyzed and discussed the maximum stress and minimum fatigue life at the corresponding position. The variation trend of stress and fatigue life at the corresponding position after fillet optimization was also discussed. The results showed that the equivalent stress of autoclave teeth without fillet optimization reached the maximum under different fillet sizes. The equivalent stress and fatigue life of the autoclave tooth were the same as the rounded corner size obtained by the optimization design. The optimal global solution could be obtained through the optimization design process.

1. Introduction

The autoclave is a special pressure device consisting of an autoclave body, autoclave body flange, autoclave cover, autoclave cover flange, swing device, and safety device. It is also widely used in industries requiring high-temperature and high-pressure processing, such as metal smelting, chemical fiber production, heating concrete pipe piles, gray sand bricks, microporous calcium carbonate, and asbestos slabs [1–7]. In order to quickly implement repeated operations such as rotation, boosting, steaming, depressurization, and unwinding during material loading and unloading, autoclaves generally have a pass-through or snap-on fast-opening structure. However, the autoclave works in a working environment with frequent changes in temperature and pressure parameters and multiple opening and closing times. The force on the autoclave tooth is constantly changing, leading to a significant reduction in the strength and service life of the autoclave and the occurrence of cracks in the autoclave tooth, as shown in Figure 1. According to incomplete statistics in some areas of Guangdong Province, the proportion of cracks in autoclaves with a nine-year expiry date is as high as 40% [8]. Some autoclaves were found to have cracks of varying degrees in 90% of flange teeth shortly after they were put into use. Cracks can easily lead to the failure of the autoclave tooth, posing a serious threat to the safety of the autoclave [9]. How to avoid production accidents due to the reduction of the autoclave tooth crack? Many scholars and engineers have investigated the properties of autoclaves due to their widespread use in multiple filing devices.

In terms of the fluid flow and heat transfer of the autoclave, Shi et al. adopted the finite element method to discuss the jacketed poly-condensation autoclave and solve the leakage problem [10]. Joshi and Archarya used the finite element method to discuss the combined effect of different parameters on the autoclave [11]. Du et al. analyzed the stress and temperature of the autoclave and verified its simulation with the experimental result [12]. Li et al. investigated an industry-size autoclave with an aspect ratio of 10 about the three-dimensional heat transfer and fluid flow in hydrothermal growth due to such nonuniform heating [13]. Bohne et al. proposed a numerical method to observe heat transfer in a small laboratory autoclave using

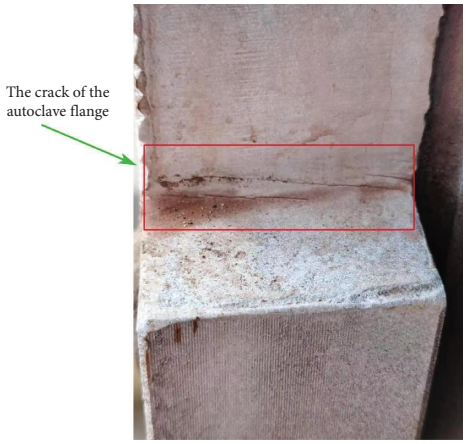

Figure 1: Crack at the root side of the autoclave flange tooth.

calorimeter measurements and a fluid dynamic model [14]. Zhu et al. utilized a quasi-transient coupling approach to model the heat transfer in the autoclave, which reduces the computational cost and high correlation [15]. Lau et al. extended the previously numerical methodology developed to simulate in detail the thermal energy consumption of an industrial-sized empty autoclave used for steam sterilization [16]. Sun et al. proposed three optimization schemes for the autoclave problem of uneven air inlet flow to improve the flow-field characteristics [17]. Kluge et al. investigated the temperature distribution on an industrial mold tool monitored during autoclave runs with three settings [18]. Dolkun et al. investigated the influence of mold placement variation in an autoclave on the heating performance of a large framed mold and found the optimal mold placement parameters for improving the temperature uniformity and heating rate [19]. Weber developed a semiempirical approach for boundary condition estimation that enables a simple and fast thermal simulation of the autoclave curing process with reasonably high accuracy [20]. Xie et al. found that increasing the time of heat preservation and the number of periods could improve uniformity significantly [21]. Although the autoclave's fluid flow and heat transfer are thoroughly discussed, the crack of the autoclave and the problem of relative parameters design are ignored.

Apart from the discussion of the heat transfer and the fluid flow of the autoclave, the strength analysis of the autoclave under specific working conditions also has attracted more and more researchers' attention. The autoclave tooth and flanges without thermal insulation treatment have an evident temperature gradient bound to cause enormous thermal stress [22]. The autoclave is under the action of alternating thermal stress and pressure load for a long time, and a low-cycle fatigue trend can be determined when the number of alternating cycles exceeds 1000 [23]. The right-angle part of the tooth root with the most severe stress concentration is subjected to tremendous shear stress, and fatigue cracks are generated and spread under the action of long-term alternating stress [24]. Dong and Kang discussed the stress and deformation of the door shaft of the autoclave by using the finite element method and measured the corresponding experimental data by using electrical measurement method to verify the credibility of the calculation results [25]. Wu simulated the contact process of the autoclave cover and body with the face-surface element in Ansys, evaluated the structural strength of the autoclave, and verified the reliability of the structural design of the autoclave based on the numerical method [26]. Aiming at the network crack problem in the autoclave, Lei analyzed the crack generation location and crack and discussed the related cause [27]. Su et al. adopted the parametric modelling method in Pro/E and Ansys workbench to optimize the wall thickness design of an ultralarge autoclave vessel with a diameter of 4 m, which improved the efficiency of design calculation, ensured the structural strength, and effectively reduced the consumption of autoclave manufacturing materials [28]. Lu et al. analyzed the stress corrosion cracks, cold cracks, fatigue cracks, and the causes of the cracks in the base metal, weld, and kettle teeth of the autoclave [29]. Chen listed some common defects found in regular inspection of autoclaves in production, such as cracks, corrosion, deformation, and safety interlock failure, and made a preliminary analysis of these reasons [30]. Besides, the use of the finite element method (FEM) for the estimation of fatigue life under variable amplitude loading has been proved as a good alternative to experimental methods [31]. The duralumin aircraft spar fatigue life is evaluated by the extended finite element method (XFEM) under cyclic loading conditions [32]. Aleksandar and Bosko used the finite element method for fatigue crack growth predictions on the 2D model of the spar, whereas XFEM is used for fatigue crack growth predictions and fatigue life estimation of corresponding the 3D model [33]. Gordana et al. used a versatile and easy approximate procedure to estimate mode I stress intensity factors in case of multiple surface cracks in a three-dimensional elastic body subjected to remote uniaxial tensile loading [34].

In terms of the optimization algorithm and the optimization of the autoclave, Gu et al. utilized a multi-objective genetic algorithm to optimize the parameters of a multi-source vibration machine, the complex vibration of the combined harvester [35]. Xiao et al. proposed a novel control algorithm combining the linear quadratic regulator (LQR) control and trajectory planning (TP) to optimize a crane system [36]. Maffezzoli and Grieco proposed an optimization model derived by defining an objective function in terms of penalty coefficients associated with different tools and positions in the autoclave [37]. Weber et al. took up the experience-based tooling design approach to explain different influences on mold heat-up and how they can be covered in a thermal tooling simulation on an industrial scale [38]. Wang et al. proposed a novel multihierarchical successive optimization method to reduce the spring-back in autoclave forming [39]. Dios et al. proposed a mixed integer linear programming model to optimize the composite part placement in an autoclave [40]. Although the optimization algorithm and the optimization of the autoclave are discussed, the specific process of numerical simulation is ignored.

As seen from the above discussion, it is a crucial design step to ensure the rational structural design of the autoclave

tooth and avoid production accidents using numerical simulation. The numerical simulation presents the stress variation rule of the autoclave under operating environmental conditions, and the influence of unreasonable design parameters on its strength and service life can be avoided. Although scholars and engineers have increasingly discussed the numerical simulation method for autoclave analysis, the auto-optimized design of the autoclave has not attracted much attention using finite element analysis to calculate the strength of an autoclave. The research of the auto-optimized design for the autoclave tooth not only can avoid the production accident of autoclave but also can prolong the service life of a worth 100,000$ autoclave. The structure and performance of the autoclave can be designed and optimized by numerical simulation, including the design of the geometric shape, material selection, and pipeline layout. By adjusting the design parameters, the efficiency of the autoclave can be improved, energy consumption can be reduced, and service life can be prolonged.

In this paper, we use the stress module of Static Structure, the heat transfer module of Fluent, and the Direct Optimization module to build an autoclave finite element analysis model in the Ansys Workbench platform. The rules of the stress on the autoclave teeth are discussed through numerical calculation, and the auto-optimized design is carried out to consider the stress and fatigue life of the autoclave. It is useful for the overall safety of autoclave to optimize the relevant design of the autoclave tooth.

2. Numerical Methods and Geometrical Model

2.1. Geometrical Model. In this paper, a commonly used autoclave with an inner diameter of 2.5 m is taken as the geometrical object, as shown in Figures 2 and 3. Its structural diagram is shown in Figures 2(a) and 2(b) show the diagram of the autoclave body flange, whose overall number of autoclave teeth is 40. Figure 2(c) is the engagement diagram of the autoclave tooth, and Figure 2(d) is the simplified solid model used in numerical simulation. The structure size of the autoclave, such as autoclave flange, autoclave cover, and other parameters, is shown in Figure 3. In order to reduce the huge calculation amount brought by the huge overall structure of the autoclave, the generalized axially symmetric autoclave model is calculated by taking one-fortieth of the whole according to the periodic symmetry of the autoclave structure. The length of the simplified autoclave body is 400 mm based on the consideration of edge stress in the plate and shell theory. The nomenclature and lists of acronyms and abbreviations are presented in Table 1, and the relevant performance parameters of the autoclave are shown in Table 2. The numerical simulation and optimization of the fillet radius at the root side of the autoclave tooth are carried out according to its working characteristics to improve the design of the autoclave.

2.2. Ansys Workbench Analysis Process. In the actual production process of an autoclave, the autoclave studied in this paper undergoes the process of pressure boosting, pressure retention, and pressure drop of steam discharge. In order to save energy and improve the utilization rate of steam heat energy, it is usually used to reverse steam and boost the pressure with the remaining steam after steaming in the autoclave. Because the pressure of the steam source is relatively low, the whole pressure boost time is relatively long, which takes about 1 hour. After several hours of pressure holding (temperature), the remaining steam is finally poured out, and the product is removed when the pressure in the autoclave drops to zero.

Finite element analysis is a computer-aided engineering technique used to simulate and predict various engineering structures' stress, deformation, thermal response, and other physical behaviours under different loads. In finite element analysis, first, the structure must be discretized into many small units. Mathematical models and computer programs are used to simulate and solve the physical behaviour of each small unit. Finally, the calculation results of each small unit are combined to get the physical response of the whole structure.

In order to simulate the working of the autoclave, the analysis process of the autoclave in the paper includes two modules: (1) Fluent; (2) Static Structural, as shown in Figure 4. The structural model of the autoclave adopts 20-node Solid 186 elements of Ansys. Solid 186 elements can solve the problems of spatial anisotropy, plasticity, hyperelasticity, creep, stress toughening, large deformation, and large strain.

The module of Fluent is used to calculate the temperature distribution of the autoclave in specific boundary conditions. The flow of heat transfer calculation is rough as follows: (1) Model building: build the model according to the actual situation, including the model geometry, boundary conditions, and material properties. (2) Grid partitioning: divide the model into a finite number of small grids, and solve the physical quantities on each grid (such as temperature) by numerical methods. (3) Define the physical model: select the corresponding physical model (such as conduction, convection, or radiation) according to the specific heat transfer problem. 4. Select solver: choose a solver suitable for the problem type, such as steady-state. (5) Define the solution parameters: set the iterative convergence standard, time step, and calculation domain parameters. (6) Calculation: run the solver to calculate the physical quantities in the model, and obtain the temperature on each grid. Then, the steady autoclave temperature calculated by the Fluent is imported into the autoclave module of Static Structural for stress calculation. The stress and fatigue life of the autoclave tooth under the same temperature and pressure conditions are calculated through numerical simulation of two modules. In order to investigate the mechanical mechanism of the autoclave and reduce the calculation cost of the numerical simulation, the third module of Direct Optimization is introduced when the autoclave tooth is optimized with different fillet radius.

Direct Optimization module needs to set the input and output variables to calculate the design fillet size corresponding to the minimum equivalent stress and maximum fatigue life iteratively with a smaller fillet interval and then achieve the corresponding optimization purpose.

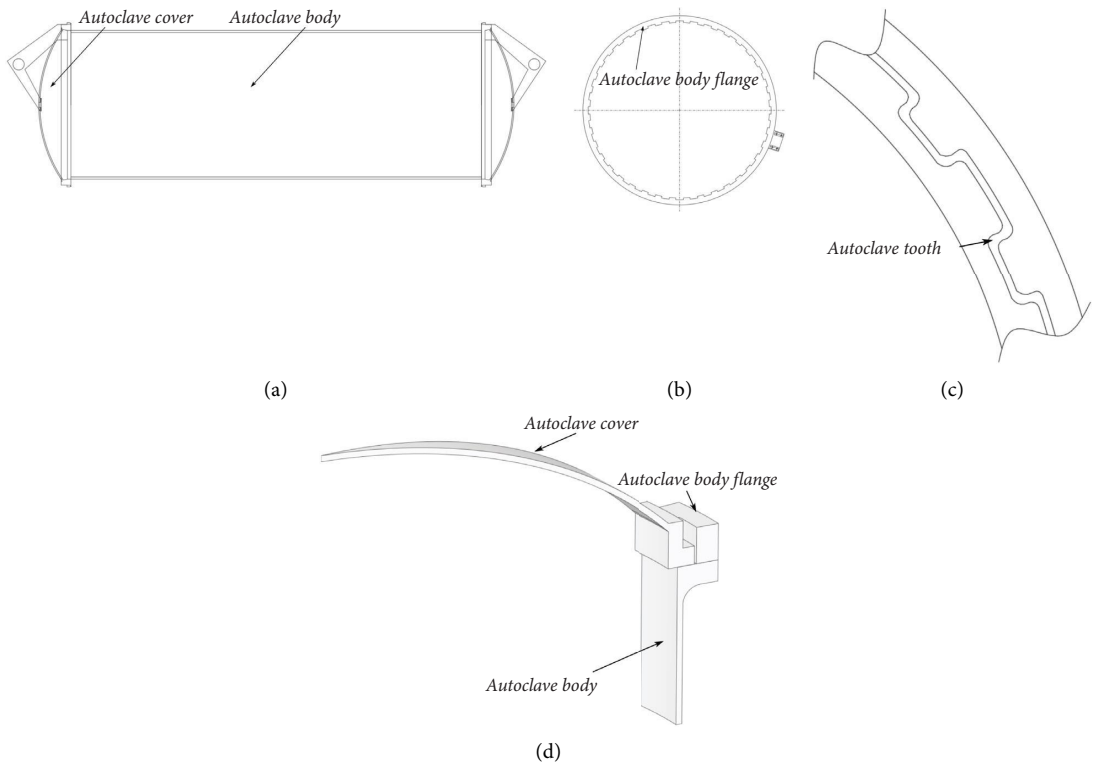

Figure 2: The diagram of the autoclave: (a) the whole body of the autoclave; (b) the diagram of the autoclave; (c) the engagement of the autoclave flange; (d) the diagram of the one-fortieth of the whole autoclave.

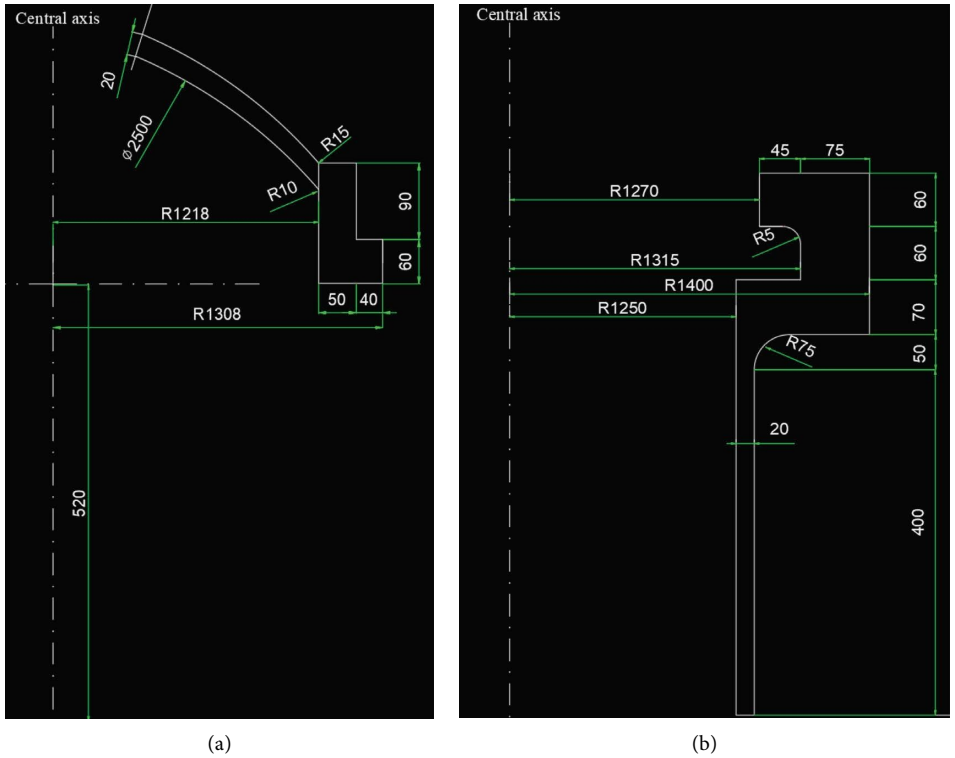

Figure 3: The geometric parameters of the autoclave: (a) the diagram of the ball-shaped head; (b) the diagram of the autoclave flange.

Table 1: The nomenclature and lists of acronyms and abbreviations.

Serial numbers	The nomenclature	The abbreviation
1	Design pressure	DP
2	Design temperature	DT
3	Working pressure	WP
4	Working temperature	WT
5	Working medium	WM
6	Megapascal	Mpa
7	Material of construction	MOC

Table 2: Main technical parameters of the autoclave.

Serial numbers	Contents	Units	Parameters
1	DP	Mpa	1.6
2	DT	˚C	204
3	WP	MPa	1.5
4	WT	˚C	201
5	WM	\	Saturated vapor
6	MOC	\	Q345R, 16Mn
7	The thickness of the plate	mm	22/26
8	The diameter of the autoclave	m	2.5

Figure 4: The flowchart of the Ansys workbench optimization.

2.3. The Equivalent Stress. In order to determine the most dangerous part at the root of the autoclave flange and the distribution and change of the stress, that is, Von Mises Stress and elastic stress concentration coefficient are used in this paper to discuss the merits of stress and design at the root of the autoclave flange with different fillet radius. The equivalent stress σ_e is calculated by (1)

$$\sigma_e = \sqrt{\frac{1}{2}\left[(\sigma_1 - \sigma_2)^2 + (\sigma_2 - \sigma_3)^2 + (\sigma_3 - \sigma_1)^2\right]}, \quad (1)$$

where σ_1, σ_2, and σ_3 are the first, second, and third principal stresses, respectively

2.4. The Energy Equation in the Autoclave. The energy transport equation of the autoclave tooth is calculated in the ANSYS Fluent as follows:

$$\frac{\partial}{\partial t}(\rho E) + \nabla\left(\vec{v}(\rho E + p)\right) = \nabla\left(k_{\text{eff}}\nabla T - \sum_j h_j \vec{J}_j + \left(\bar{\bar{\tau}}_{\text{eff}}\vec{v}\right)\right) + S_h, \quad (2)$$

where ρ is the density of the autoclave; h is the sensible enthalpy of the autoclave; k_{eff} is the effective conductivity; T is the temperature of the autoclave; S_h is the volumetric heat source; $\vec{J}_j$ is the diffusion flux of environment. The first three terms on the right-hand side of (2) represent the energy transfer of the autoclave due to conduction, species diffusion, and viscous dissipation. The second term on the left-hand (2) indicates the convective energy transfer due to the motion of the environment. The velocity field is computed from the motion specified for the autoclave.

In (2),

$$E = h - \frac{p}{\rho} + \frac{v^2}{2}, \quad (3)$$

for the incompressible flows as

$$h = \sum_j Y_j h_j + \frac{p}{\rho}. \quad (4)$$

In (4), Y_j is the mass fraction of species j and

$$h_j = \int_{T_{\text{ref}}}^{T} c_{p,j}\mathrm{d}T. \quad (5)$$

The T_{ref} in sensible enthalpy calculation is 298.15 K.

2.5. The Optimization of the Adaptive Multiobjective Algorithm. The adaptive multiobjective algorithm is an advanced optimization algorithm with the following advantages. Multiple objective functions can be processed simultaneously. Adaptive multiobjective algorithms can optimize multiple objective functions simultaneously instead of only considering one. It makes the algorithm more comprehensive and comprehensive, which can obtain better optimization results while ensuring the balance between various objectives. Adaptive parameter adjustment: adaptive multiobjective algorithms can automatically adjust parameters to adapt to optimization problems and environments. It makes the algorithm to have better adaptability and robustness. It can effectively deal with nonlinear, nonconvex, multipeak, and other complex problems: adaptive multiobjective algorithms can effectively deal with nonlinear, nonconvex, multipeak, and other complex problems, while traditional optimization algorithms often can only deal with linear or convex optimization problems. Fast convergence: adaptive multiobjective algorithm usually has the characteristic of fast convergence and can obtain better optimization results in a short time that can deal with high dimensional problems. To handle high-dimensional

problems, adaptive multiobjective algorithms can handle high-dimensional optimization problems where traditional optimization algorithms do not perform well. In conclusion, adaptive multiobjective algorithms have great advantages in multiobjective optimization problems and can achieve better optimization results.

The adaptive multiobjective algorithm is adopted to optimize the autoclave tooth. Solving a multiobjective problem is to find a set of optimal solutions when the given constraints and multiple objective function conditions are met. Its mathematical expression is as follows:

$$\begin{aligned} &\min \quad F(x) = [f_1(x), f_2(x), L, f_m(x)], \\ &\text{s.t.} \begin{cases} g_i(x) \leqslant 0, \ i = 1, 2, L, k, \\ h_i(x) \leqslant 0, \ i = 1, 2, L, p, \\ a_i \leqslant x_i \leqslant b_i, \ i = 1, 2, L, n, \end{cases} \end{aligned} \tag{6}$$

where $F(x)$ is objective function; m is the number of target functions; $g_i(x)$ is inequality constraints; k is the number of inequality constraints; $h_i(x)$ is the equality constraint; p is the number of the equality constraints; x_i is the equality constraint; a_i, b_i is the upper and lower bound of the i design variable, respectively.

2.6. The Fatigue Life Analysis. Fatigue refers to the phenomenon of fracture failure of a structure under repeated action of loads lower than the ultimate static strength. The main influencing factors of fatigue life include the number of load cycles, the stress amplitude of each cycle, the fatigue life of each cycle mean stress, and local stress concentration. The fatigue life analysis used for the numerical simulation is the nominal stress method (S-N), which is expressed as follows:

$$NS^m = C, \tag{7}$$

where m and c are the material constant; s is the autoclave stress; N is the fatigue life. S-N method is a common calculation method of fatigue cumulative damage according to Miner certainty law. The generation of fatigue damage is regarded as a deterministic event if fatigue stress amplitude is greater than the fatigue limit fatigue damage by using this method.

3. Results and Discussion

In view of the large stress concentration coefficient caused by the approximately right angle at the autoclave tooth in production practice, the paper determines to optimize the autoclave tooth with a new numerical method. Twelve sets of finite numerical element simulation experiments are set for the autoclave tooth with different fillet radii ranging from 0 mm to 22 mm. The further optimization for the optimal fillet is acquired by the variation law of the equivalent stress and fatigue life at the autoclave teeth. The process is autosolved by the mentioned analysis process.

3.1. Grid Division and Boundary Conditions. The structural model of the autoclave adopts 20-node Solid 186 elements of Ansys, which can solve the problems of spatial anisotropy, plasticity, hyperelasticity, creep, stress toughening, large deformation, and large strain. The minimum mesh size of the autoclave is 0.1 mm, and the maximum mesh size is 5 mm to ensure that there are no less than four grids in the thickness direction, as shown in Figure 5. The total number of autoclave grids was finally divided into 1.298×105. The mesh size of the autoclave heat transfer model is the same as the structural model so as to keep the geometric correspondence and avoid the error of the interpolation. The contact pair at the meshing tooth surface of the autoclave body flange and autoclave cover is set as frictional with the contact friction value of 0.3. The target surface is the autoclave body flange. The contact surface is the autoclave cover.

In the autoclave curing process for the building materials, the autoclave needs to undergo the process of pressure boost, retention, and reduction of steam discharge. Autoclaves are normally used two to three times a day. In order to save energy and improve the utilization rate of steam heat energy, the remaining steam of other autoclaves is usually used to reverse steam and boost pressure. Because the steam source pressure is relatively low, the whole pressure boost time is about 1~2 hours long. Then, after holding constant temperature and pressure for about 6~8 hours, the remaining steam is poured out. The product is removed when the pressure in the autoclave drops to zero. The paper mainly discusses the process of pressure retention with constant temperature and pressure. The heat transfer boundary condition is set according to the autoclave production condition, as shown in Figure 6. As the autoclave calculation model is simplified to one-fortieth of the original one, the boundary conditions of autoclave in Static Structural (ANSYS) impose symmetric constraints on the symmetric planes on both sides of the autoclave according to the characteristics of the generalized axial symmetry problem. The axial displacement constraint on the autoclave cover and the lower end of the autoclave body is 0, as shown in Figure 7. According to the actual operation condition of the autoclave, a uniform pressure load of 1.5 MPa is applied to the inner surface of the autoclave body and cover.

3.2. The Verification of the Numerical Simulation and Grid Independence. In order to verify the reliability of the finite element method in calculating the stress of the autoclave, the stress at the autoclave tooth in numerical simulation is compared with the experimental result, as shown in Figures 8(a)–8(d). Figure 8(b) presents the autoclave of the experimental test. Figure 8(c) presents the data collection of the static strain gauge, and Figure 8(d) presents the distribution of the static strain gauge around the autoclave tooth.

Considering that the surface temperature of the autoclave body flange is close to 200°C when the autoclave is in use, the high-temperature resistant the BAB120-3AA strain gauge with ten static channel strain gauge YSV8310 is adopted. The operating temperature range of BAB120-3AA strain gauge is −200°C~250°C, which can meet the requirements of the on-site autoclave stress test. The specific site environmental conditions are as follows: weather: fine;

Figure 5: The grid division of autoclave.

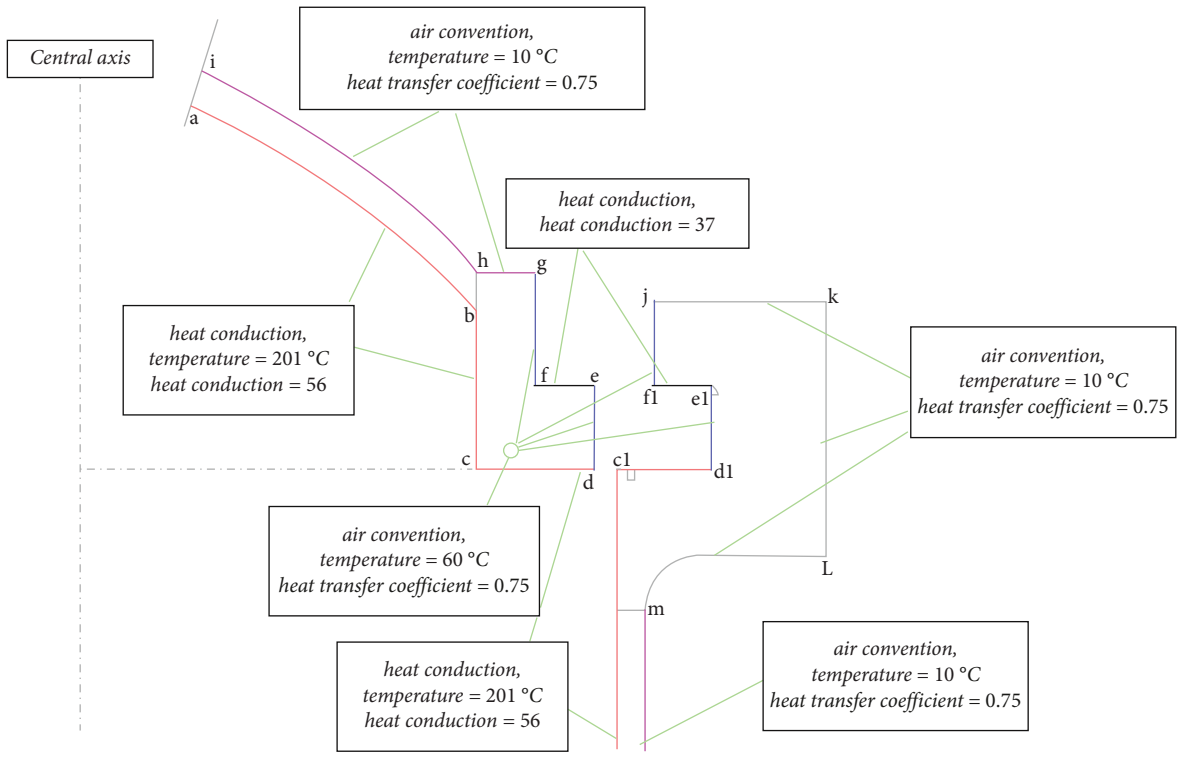

Figure 6: The heat transfer boundary condition of the autoclave in Fluent.

temperature: 10°C; wind: north wind level: 2~3; humidity: 58%; working pressure: 1.5 MPa, pressure holding time: 2 + 8 hours; site environment: indoor. The part of the experiment is the inner surface between the autoclave teeth of 25~26 and 27~28 (directly opposite the autoclave flange, starting at 12 o'clock and counting in a clockwise direction). A total of 8 strain gauges are attached in the cold state.

The direction of the equivalent stress is radial, not in the expansion plane of the main crack at the root of the tooth side. The macroscopic fatigue crack generally expands in the maximum tensile stress plane, so the influence of the equivalent stress on the fatigue crack is not considered. The experiment starts from the autoclave booster to depressurized discharge. Although each strain gauge collects a large

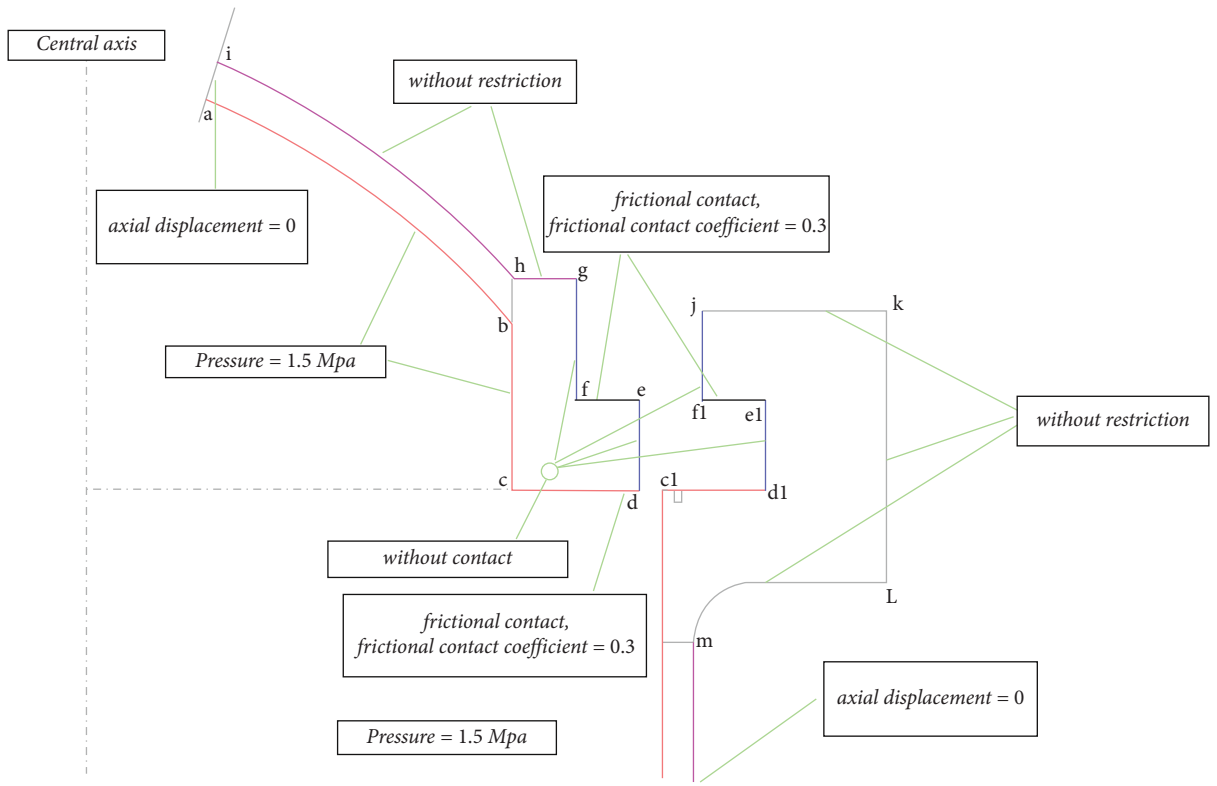

Figure 7: The structural condition of the autoclave in Static Structure.

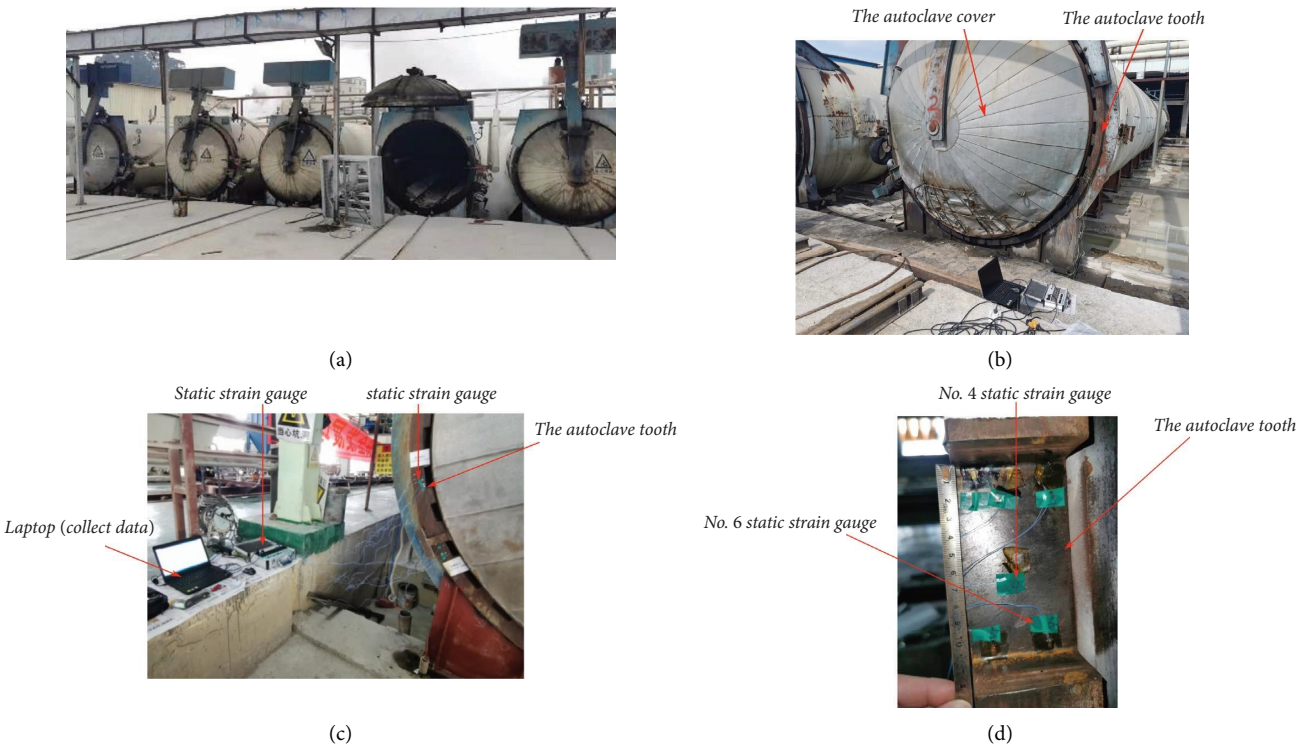

Figure 8: The diagram of the experiment: (a) the whole test plant; (b) the autoclave; (c) the equipment of the experiment; (d) the distribution of the strain gauges.

amount of data, the measured data in some of them change little. Therefore, the representative No.4 and No.6 strain gauges are selected. The measured stress results are shown in Figures 9(a) and 9(b); the stress curve measured by the No.4 and No.6 strain gauge after smoothing fitting is shown in Figure 9(c). It is obvious from the test results that the inner surface of the autoclave is subjected to tensile stress and changes periodically with the pressure in the autoclave. The paper mainly investigates the stress of the autoclave in pressure retention (10000~20000 s). The average value of the No.4 strain gauge at the autoclave tooth is 250.439 N, and the average value of the No.6 strain gauge at the autoclave tooth is 256.47 N.

In order to ensure the grid independence of the numerical simulation, the total mesh used for the numerical simulation is refined from the number of 8.32×104 of course mesh increases to 1.29×105 of the middle mesh and 2.47×106 of the fine mesh. The stress of the numerical simulation at the autoclave tooth in the different mesh is compared with the No.6 strain gauge. The numerical result of the stress and relative errors compared with the No.6 strain gauge is presented in Table 3. The relative error of the numerical result is calculated by the experimental result of No.6 strain gauge stress.

As shown in Table 3, it can be found that the relative error about numerical result pr first decreases and then increases when the number of mesh increases. The relative errors show a slight difference when the middle mesh is refined to the fine mesh. The calculation accuracy of the middle mesh of the autoclave has reached the requirement for the autoclave simulation. In order to keep the efficiency of the numerical simulation, the middle mesh is used to simulate the autoclave.

3.3. The Temperature Analysis of the Autoclave. The thermal stress caused by the temperature in the autoclave is so significant that the distribution temperature of the autoclave has to be calculated precisely. The experimental surface temperature of the autoclave tooth is detected by a Fluke TiX580 handheld infrared thermal imager, as shown in Figure 10. Figure 10 shows the radial thermal image distribution of the side of the autoclave flange when the autoclave is heated for 20 min. It can be seen that the temperature difference is about 48°C in the radial direction (the thickness direction of the autoclave) of the surface of the autoclave flange.

The temperature distribution of the autoclave is high in the middle along the radial direction and low on both sides inside and outside. Along the axis, the inner is high, and the outer edge is low. The reason for the temperature distribution of the autoclave is presented as follows.

The inner end of the autoclave flange is welded with the autoclave body, and a thermal insulation layer covers the connecting part. When the autoclave is heated by steam, its inner side is subjected to the heat conduction of the heated autoclave body. The heat transfer of the steam contact is equivalent to the internal heat source at the inside autoclave flange. The temperature in the internal heat source is constantly changing with the change of steam pressure. Under the heating action of the heat source inside the flange, the heat conducts heat along the axial direction of the autoclave body to the outside of the autoclave flange. According to the thermal insulation monitoring of the autoclave flange, it can be found that the inner and outer surfaces of the autoclave flange and the outer surfaces of the autoclave without thermal insulation are in contact with the air. When the temperature of the autoclave flange rises, it can carry out convection and radiation heat transfer with the environment (air). The autoclave flange acts as fins in the process of the heat transfer, improving the heat transfer.

In the initial stage of autoclave heating, when there is no heat transfer at the flange surface, the temperature in the metal of the flange gradually decreases along the heat transfer route. As the heating process further develops, the surface heat transfer from the autoclave flange gradually increases. When the autoclave pressure rises to the rated pressure, the steam temperature no longer changes and can be regarded as a stable internal heat source. Under the action of this heat source, when the heat conduction reaches a certain depth, the influence of the above initial temperature distribution gradually disappears and enters the normal stage of unsteady heat conduction. The thermal boundary conditions mainly affect the temperature distribution at different times until the autoclave depresses.

The temperature distribution of the autoclave and the cross section at the autoclave flange are shown in Figures 11(a)–11(b). As can be seen from the temperature contour, most of the autoclaved temperature is 201°C after the steam is passed into the autoclave. The temperature difference inside and outside of the autoclave is around zero after calculating the steady state. This is because there is no insulation in this part, but there is a distinct temperature difference in the meshed part of the autoclave flange. According to the variation law of the temperature gradient, it can be inferred that there will be a large stress around it, which leads to cracks in the root of the autoclave flange. The temperature difference in the meshed part of the autoclave flange ranges from 63.9°C~132°C, which is close to the experimental surface temperature of the autoclave tooth detected by a Fluke TiX580 handheld infrared thermal imager.

3.4. The Stress Analysis of the Autoclave Tooth. The maximum equivalent stress at the autoclave tooth line chart under different fillet radii is presented in Figure 12. With the increase of the fillet radius at the autoclave tooth, the maximum equivalent stress first decreases and then increases, indicating there is an optimal fillet radius for the design of the autoclave tooth. The maximum equivalent force at the autoclave teeth without fillet treatment reached 252.44 MPa, while the maximum equivalent stress at the side of the kettle teeth with 12 mm fillet treatment was only 156.72 MPa. It can be found that the maximum equivalent stress amplitude decreased by about 37.91% when the autoclave tooth was designed with a 12 mm fillet radius. The reason why the stress first decreases and then increases with the increase of

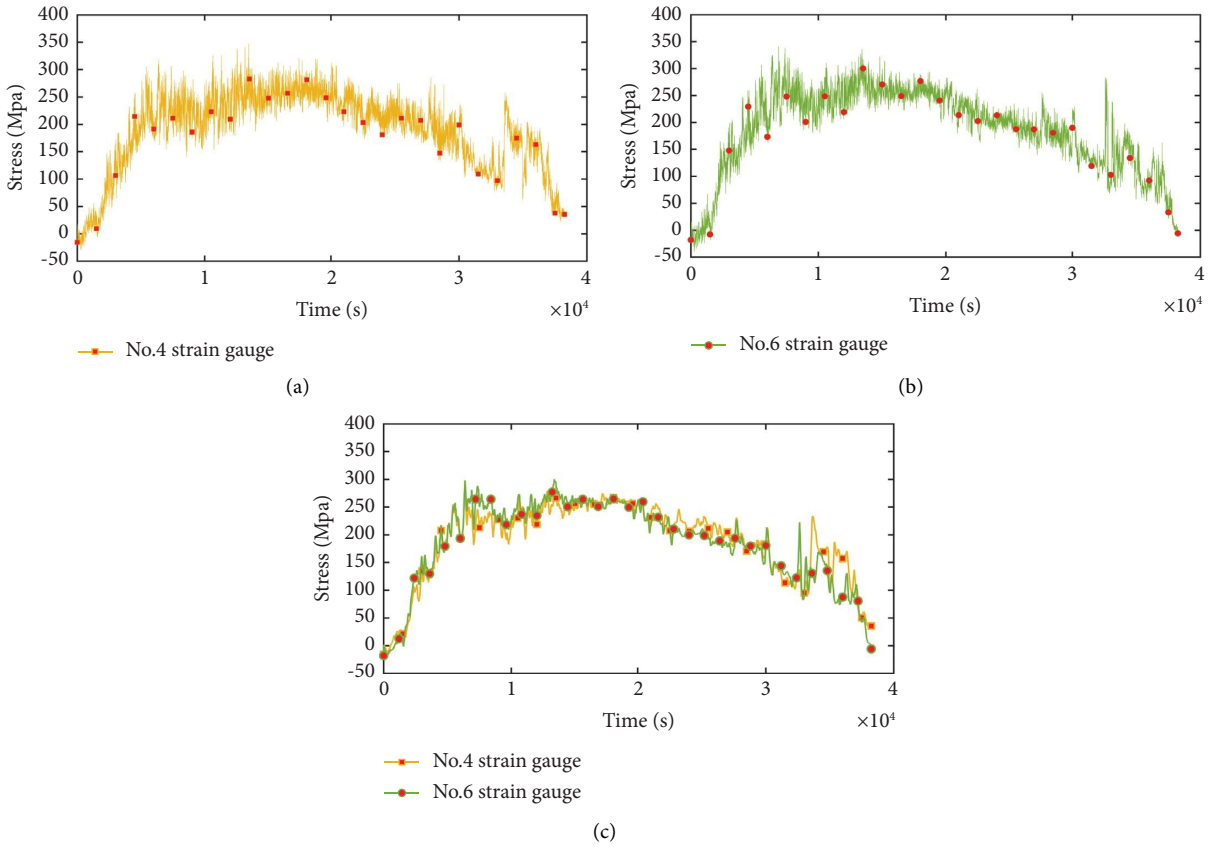

Figure 9: The experiment result of the strain gauge: (a) the experimental result of the no.4 strain gauge; (b) the experimental result of the no.6 strain gauge; (c) the numerical filter result of the no.4 and no.6 strain gauges.

Table 3: Main technical parameters of the autoclave.

Mesh	No.6 strain gauge stress	Numerical stress	Relative error
Coarse	256.47	243.76	−4.95%
Middle	256.47	252.44	−1.57%
Fine	256.47	253.28	−1.24%

the fillet radius of the autoclave tooth can be explained by the stress distribution and geometry:

First, before the fillet radius increases, there is a sharp Angle on the tooth side, leading to stress concentration and a larger stress value. When the fillet radius increases, the Angle becomes smoother, and the stress concentration degree decreases, so the stress value will also decrease. However, as the fillet radius continues to increase, the radius of the arc becomes larger compared to the curvature radius of the tooth side, resulting in the arc becoming the dominant geometry of the tooth side. At this point, the geometry of the arc begins to have a significant effect on the stress. Specifically, when the fillet radius increases to a certain extent, the curvature radius of the arc begins to be close to or less than the curvature radius of the tooth side, which makes the transition area between the tooth side and the arc become sharper. The stress concentration degree increases again, so the stress value will also increase.

Therefore, when the fillet radius increases, the stress decreases first and then increases because of the comprehensive influence of the change of fillet radius on the stress distribution and geometry. The size of the fillet radius should be balanced in terms of stress and geometry to obtain the best design results.

Increasing the radius of the tooth side fillet will increase the manufacturing cost of the autoclave. This is because, during the production process, the tooth side needs to be processed and trimmed several times to make it meet the required geometry and surface quality. With the increase in fillet radius, the difficulty and complexity of these machining and finishing procedures will also increase, resulting in an increase in production costs. In addition, increasing the fillet radius may also lead to an increase in the material cost of the autoclave. This is due to the need to select materials with higher strength and wear resistance to adapt to greater stress and harsher working environments, which increases material costs during material selection and procurement.

Figure 13 shows the contour of the maximum equivalent stress at the autoclave tooth with different fillet radii. The maximum stress value of the autoclave mainly appears at the root position of the autoclave tooth, which is different from the crack occurrence position in the production inspection. The location of the crack does not match the weakest position in the numerical simulation results, which may be due to several reasons. First, the model used in numerical

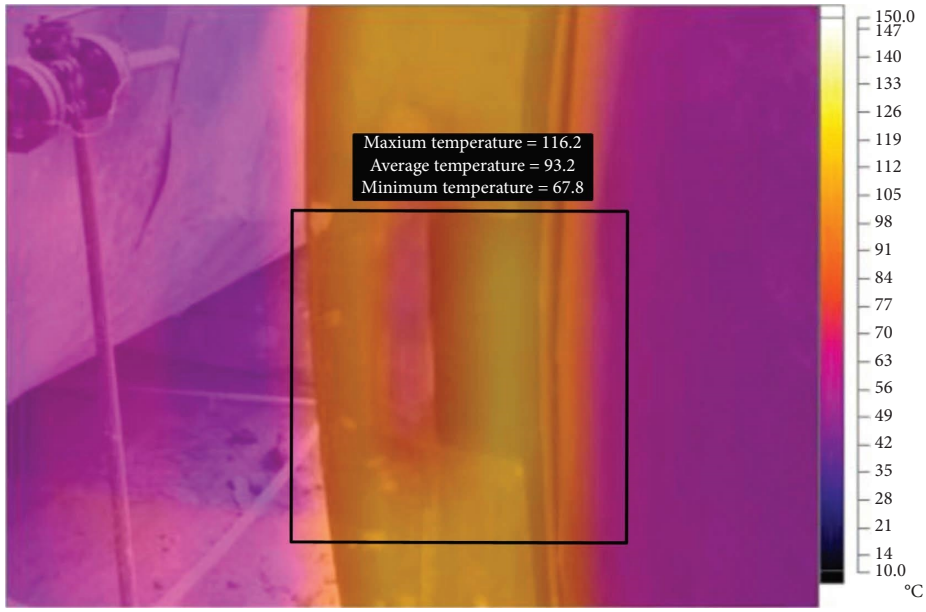

Figure 10: The radial thermal image distribution of the autoclave.

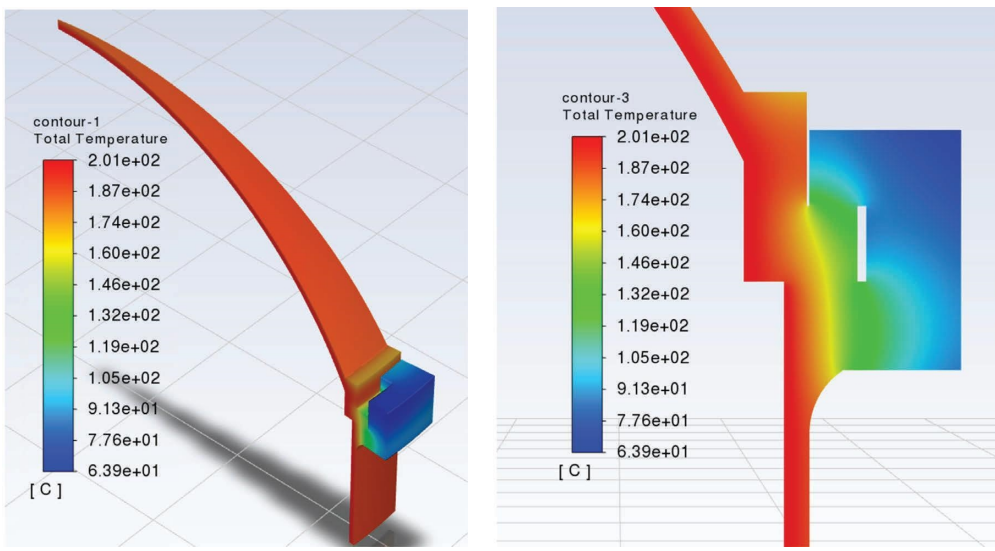

(a) (b)

Figure 11: The temperature contour of the autoclave: (a) the temperature contour of the whole autoclave flange; (b) the temperature contour of the cross-section of the autoclave.

simulation is usually a simplified version of the whole system, which may result in some differences between the model and the actual system. In the numerical simulation of the autoclave, the fracture location prediction may not be accurate enough due to the model simplification, leading to a mismatch with the actual situation. Second, material inhomogeneity may also contribute to the mismatch. The autoclave is subjected to high-temperature and high-pressure environments, and the thermal expansion and stress distribution of the material may be uneven, resulting in cracks in unexpected locations. If the numerical simulation does not consider the material inhomogeneity, the prediction results may be biased. Therefore, the mismatch between the fracture location and the weakest position in the numerical simulation results may be caused by multiple factors. Finally, it is worth noting that the generation and propagation of a local crack in the autoclave tooth is one of the main reasons for the structural failure of the autoclave. The contour of the maximum equivalent stress at the autoclave tooth verifies the reliability of the numerical

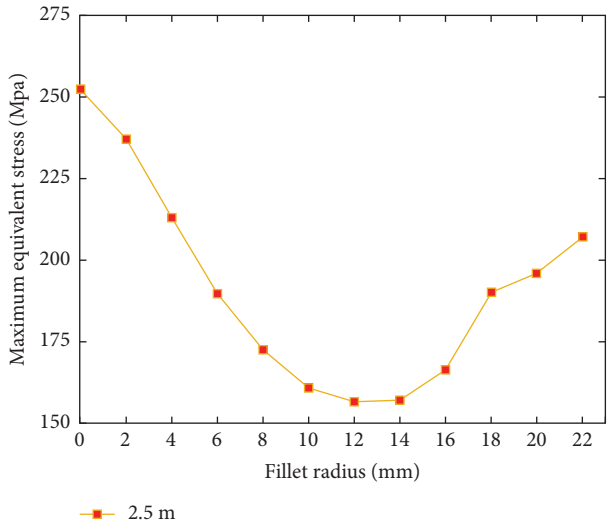

Figure 12: The maximum equivalent stress at the autoclave tooth under different fillet radii.

simulation and explains the necessity of optimization for the autoclave tooth.

3.5. The Fatigue Life of the Autoclave Tooth. The material property of the autoclave flange is selected as 16Mn, its tensile strength is 535 MPa, and its yield limit is 335 MPa. According to the above maximum equivalent stress numerical simulation and analysis, it can be known that the maximum equivalent stress at the autoclave tooth is less than the yield limit of the material. In this case, there will be no strength failure at the autoclave tooth. It can be inferred that the insufficient fatigue life of the autoclave tooth is one of the reasons for the cracks in the autoclave.

Figure 14 presents the contour of the fatigue life at the autoclave tooth with different fillet radii. It can be found that the minimum fatigue life of the autoclave tooth first increases and then decreases with the increase of fillet radius at the autoclave tooth under the cyclic effect of equal force. When the fillet is 14 mm, the fatigue life of the autoclave tooth is 62178 times, which is about six times more than that of 11358 times at 0 mm. Figure 15 shows the minimum fatigue life of the root parts of autoclaved kettle teeth with different fillet angles. It can be seen that under the same working condition, the position of the minimum fatigue life of autoclave tooth with different fillet radii is basically consistent with the position of the maximum equivalent stress. The fillet radius design for the autoclave is vital for the improving the service life at the autoclave tooth.

3.6. The Autooptimization Fillet Design of Autoclave Tooth. In this section, the paper elaborates on the optimization design process of the autoclave tooth. The specific process is shown in Figures 16 and 17. Direct Optimization is a module that searches for optimal design points based on the functional relationship between input and output variables. Based on the module, the adaptive multiobjective algorithm is selected to solve this module to find the point where the stress on the autoclave tooth is the minimum and the fatigue life on the autoclave tooth side is the maximum. It finally realizes the optimization design of the tooth root fillet of autoclave tooth.

The first step is to set the fillet of the autoclave tooth as the input variable in Direct Optimization and set the stress on the autoclave tooth and the fatigue life on the autoclave tooth side as the output variable, respectively. The second step is to set the upper and bottom limitations of the autoclave tooth fillet according to the fillet range of 10~16 mm corresponding to the maximum equivalent stress and minimum fatigue life on the autoclave tooth calculated in the previous section. Step 3 sets the optimization goal of the stress and fatigue life of the autoclave tooth side. The optimization goal of the stress at the autoclave tooth is to find the minimum value, and the fatigue life is to find the maximum value. Since the autoclave tooth's minimum stress and maximum fatigue life have not been determined, the upper and lower values of its constraint conditions can be ignored here. In the fourth step, the number of iterations in autooptimization is set as 9, and the total number of design points representing the estimated fillet radius of the autoclave tooth is obtained. Then, the computation of all design points is calculated.

The iterative results of the optimization design of the autoclave tooth under different fillet radii are shown in Figure 18. The triangle points represent the equivalent stress of the autoclave tooth when the fillet radius is adjusted, while the blue line is a fitted curve based on the distribution of the triangle points. It can be seen that the equivalent stress at the design point in the range of 10–14 mm shows a decreasing trend, and the equivalent stress at the design point in the range of 14–16 mm shows an increasing trend. In addition, the results of the adaptive multiobjective algorithm to solve the minimum equivalent stress of the design points under different fillet radii show that the distribution of the design points is more uniform in the range of 10~14 mm and 15~16 mm. In contrast, the distribution is more concentrated in the range of 14 mm~15 mm, indicating that the optimal solution of the optimization design is located in the range of 14 mm~15 mm.

Figure 19 presents the iterative fatigue life of the optimization design of the autoclave tooth under different fillet radii. The triangle points represent the fatigue life of the autoclave tooth when the fillet radius is changed, while the blue line is a fitted curve based on the distribution of the triangle points. It can be seen that the equivalent stress at the design point in the range of 10–14 mm shows an increasing trend, and the equivalent stress at the design point in the range of 14–16 mm shows a decreasing trend. In addition, the results of the adaptive multiobjective algorithm to solve the maximum fatigue life of the design points under different fillet radii show that the distribution of the design points is more uniform in the range of 10~14 mm and 15~16 mm. In contrast, the distribution is more concentrated in the range of 14 mm~15 mm, indicating that the optimal solution of the optimization design is located in the range of 14 mm~15 mm.

Therefore, the optimal fillet size of the autoclave tooth can be determined to be 14 mm, combined with the discussion of the minimum equivalent stress.

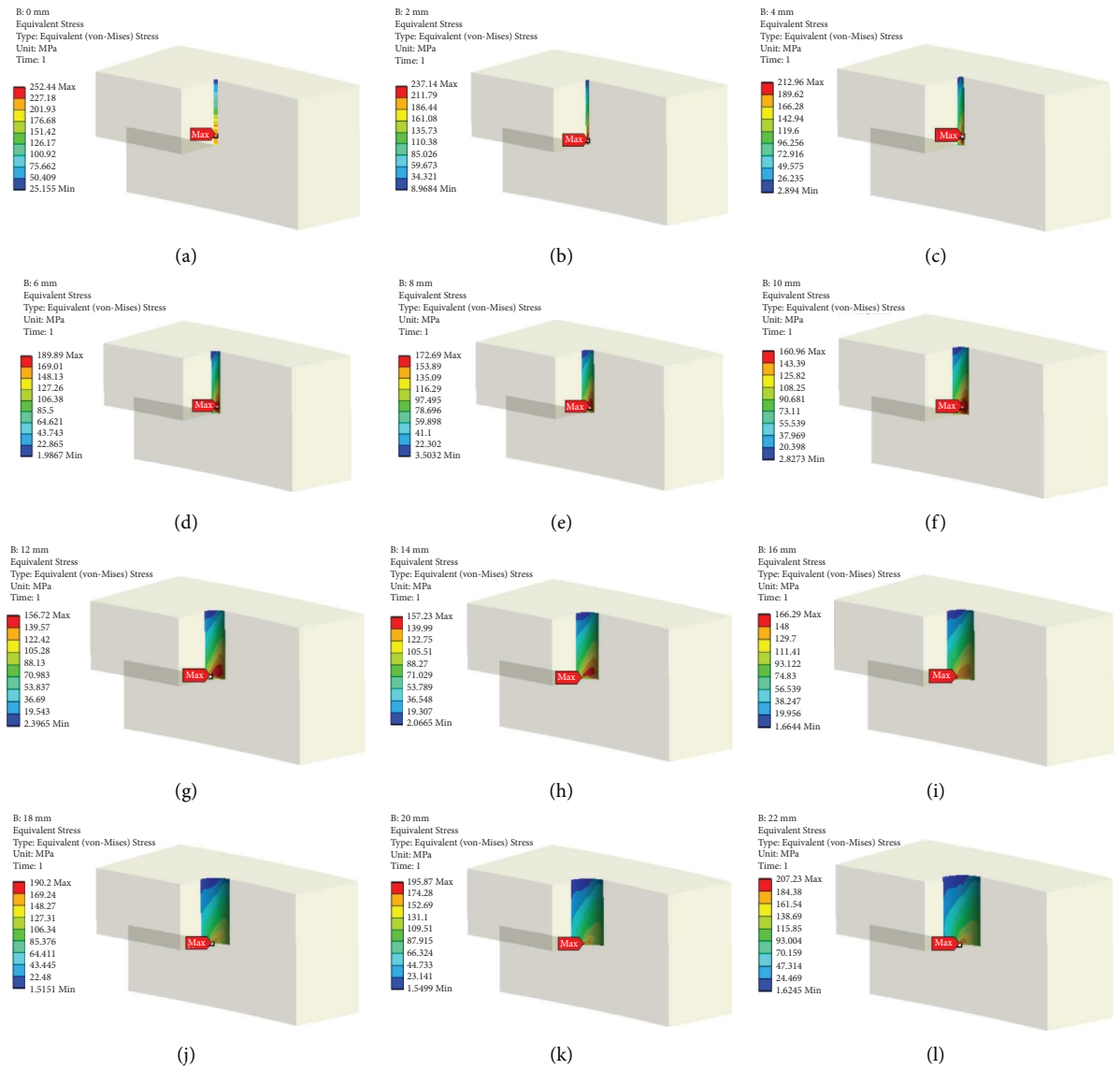

FIGURE 13: The maximum equivalent stress contour of the autoclave tooth under different fillet radii: (a) 0 mm, (b) 2 mm, (c) 4 mm, (d) 6 mm, (e) 8 mm, (f) 10 mm, (g) 12 mm, (h) 14 mm, (i) 16 mm, (j) 18 mm, (k) 20 mm, (l) 22 mm.

3.7. The Elastic Stress Concentration Coefficient of Autoclave Tooth. Aiming at the situation that the large elastic stress concentration coefficient of the autoclave tooth when the autoclave tooth is not optimized, the section discusses the stress concentration coefficient based on the Ansys stress linear tools. The elastic stress concentration coefficient K_t is calculated by (3), as shown in Figure 20.

$$K_t = \frac{\sigma_{\max}}{\sigma_m}, \tag{8}$$

where $\sigma_{\max}$ is the maximum stress value, and σ_m is the membrane stress. The membrane stress is the stress component evenly distributed along the thickness of the autoclave flange, which is equal to the average stress at the interface of the autoclave flange. It can be calculated by the following formula:

$$\sigma_m = \frac{1}{t}\int_{-t/2}^{t/2} \sigma \mathrm{d}x_m, \tag{9}$$

where t is the thickness of the autoclave flange section, σ is the total stress across the section path, and x_m is the coordinates of a point across the section path. Figures 20(a) and 20(b) show the calculation path diagram of the stress coefficient used in the numerical simulation.

The elastic stress concentration coefficient at the autoclave tooth line chart under different fillet radii is shown in Figure 21. As the increase in the fillet radius at the autoclave tooth, the elastic stress concentration coefficient first decreases and then increases, which indicates that there is an optimal fillet radius for the design of the autoclave tooth. The elastic stress concentration coefficient at the autoclave teeth without fillet treatment reached 6.35, while the elastic stress concentration coefficient at the side of the autoclave teeth

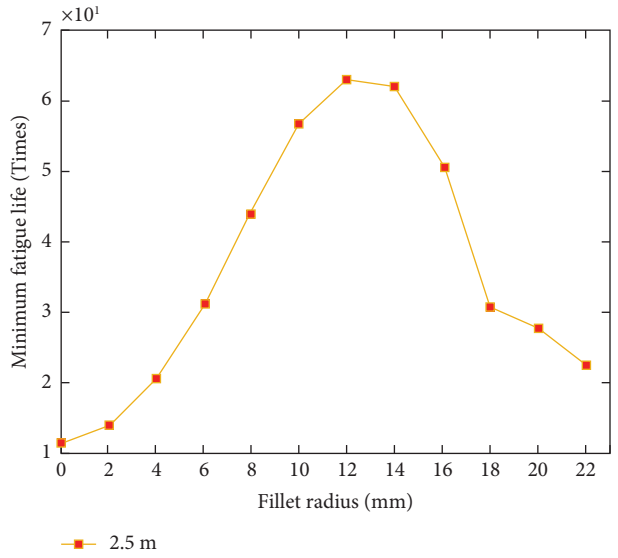

Figure 14: The fatigue life at the autoclave tooth under different fillet radii.

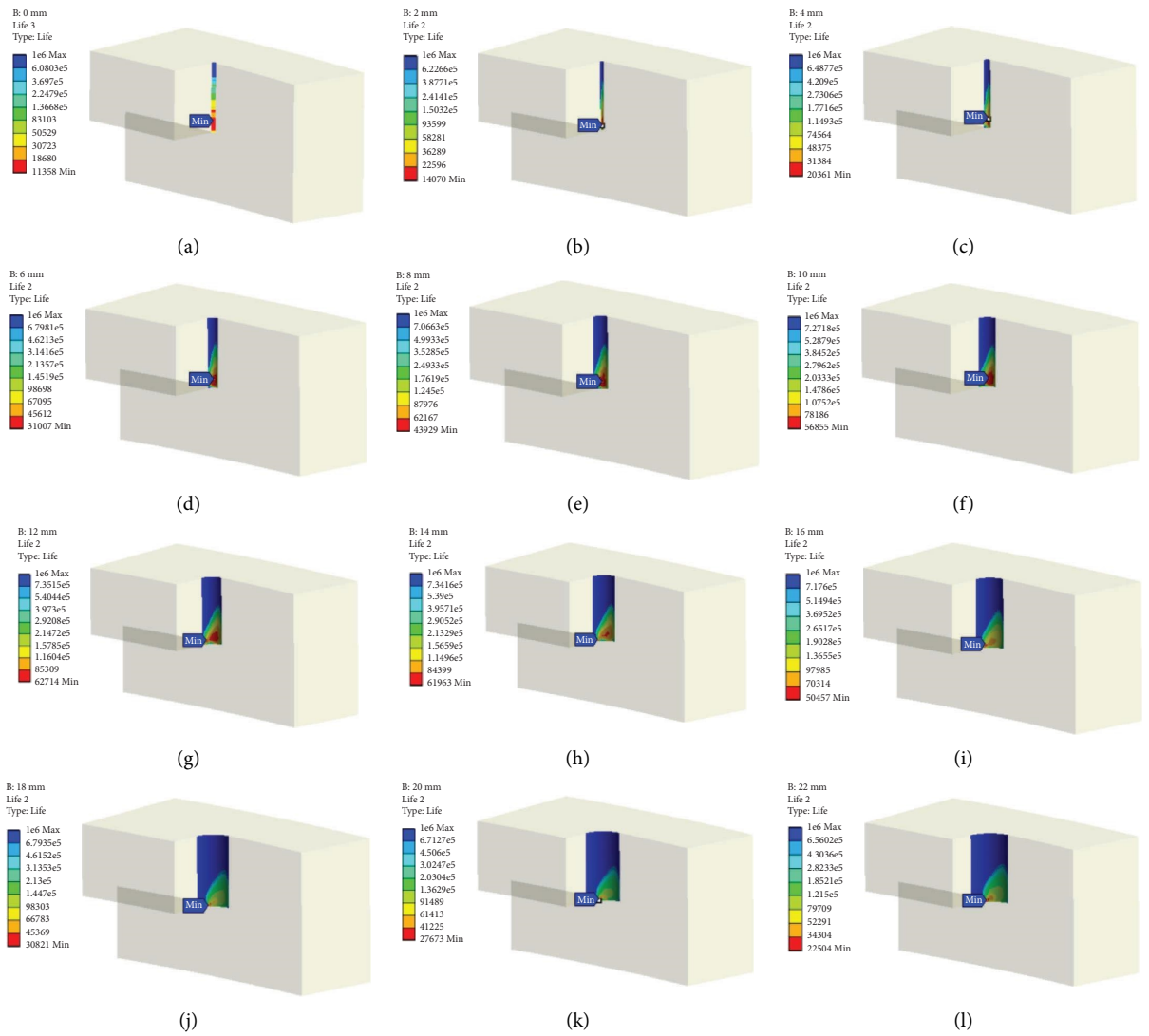

Figure 15: The fatigue life contour of the autoclave tooth under different fillet radii. (a) 0 mm, (b) 2 mm, (c) 4 mm, (d) 6 mm, (e) 8 mm, (f) 10 mm, (g) 12 mm, (h) 14 mm, (i) 16 mm, (j) 18 mm, (k) 20 mm, and (l) 22 mm.

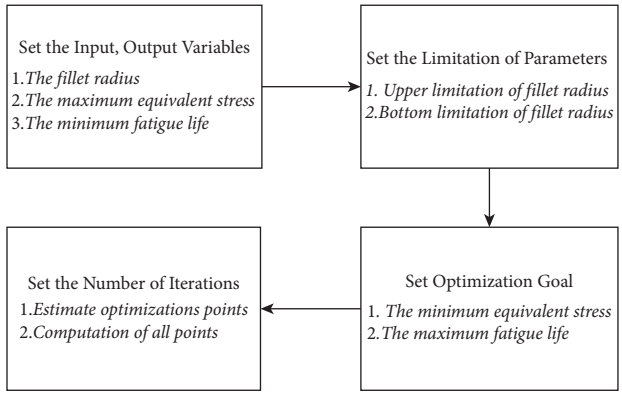

Figure 16: The optimization process of the autoclave tooth.

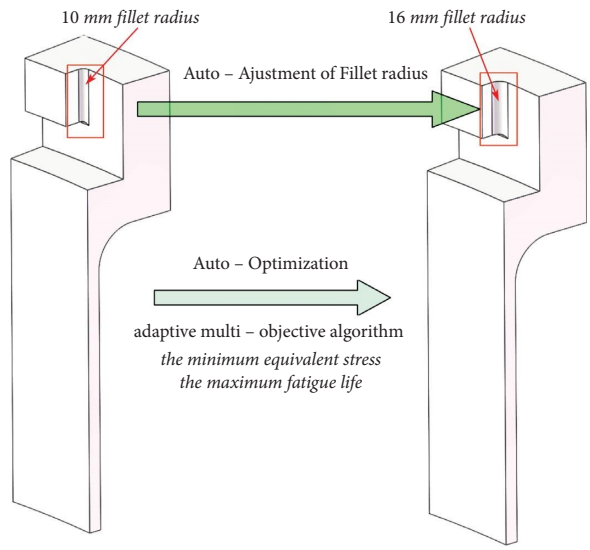

Figure 17: The optimization diagram of autoclave tooth.

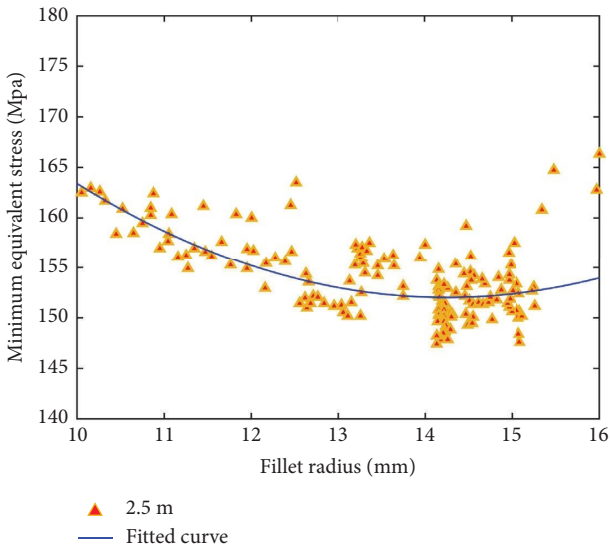

Figure 18: The equivalent stress at the autoclave tooth under different fillet radii.

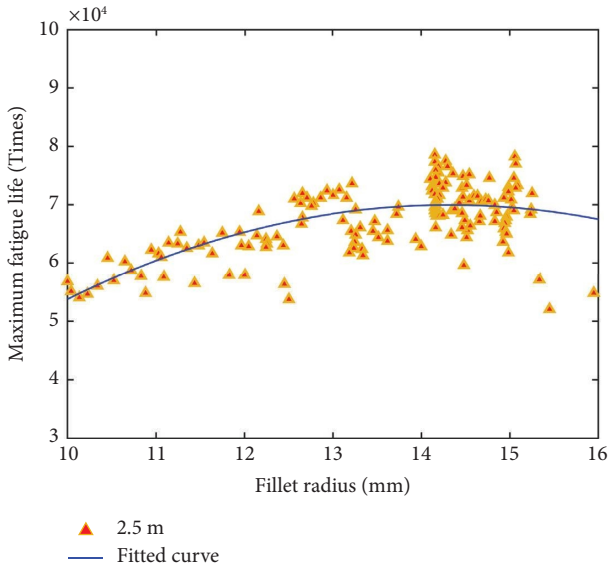

Figure 19: The fatigue life at the autoclave tooth under different fillet radii.

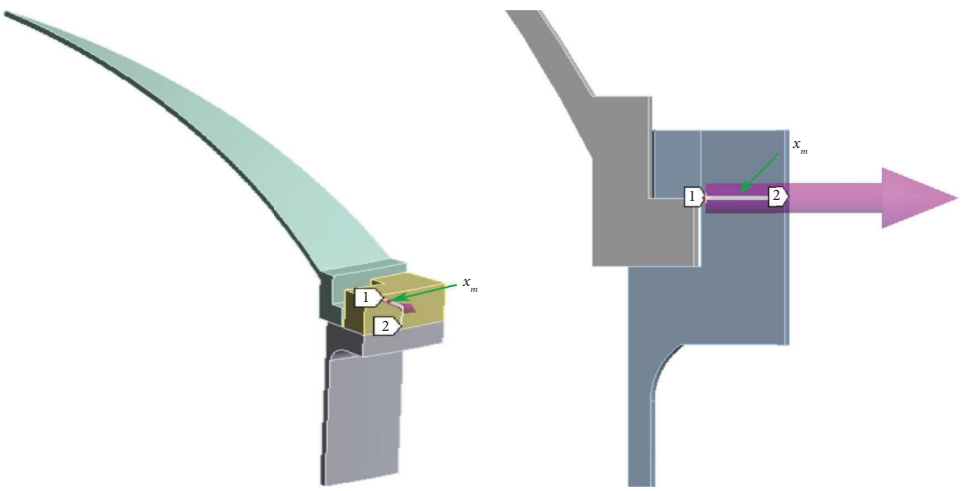

Figure 20: The diagram of the autoclave tooth stress coefficient: (a) entirety; (b) the cross section of the autoclave.

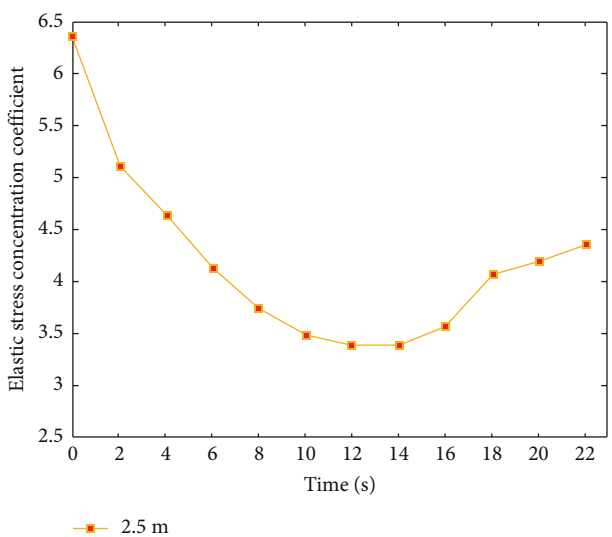

Figure 21: The elastic stress concentration coefficient at the autoclave tooth under different fillet radii.

with 12 mm fillet treatment was only 3.39. Therefore, the optimal fillet design of the autoclave tooth can effectively reduce the elastic stress concentration coefficient at the root of the autoclave tooth.

4. Conclusions

Based on the actual production, the numerical simulation flow of the Ansys workbench for the optimal design of autoclave teeth was proposed in this paper. The causes of the lateral cracks of the autoclave tooth are analyzed and discussed, as well as the variation trend of the lateral equivalent stress and fatigue life of the autoclave tooth under different radii. In order to simulate the overall temperature change of the autoclave in production, the Fluent module in Ansys is used in this paper to calculate the overall temperature of the autoclave according to the practical boundary conditions. On the Ansys Workbench, the overall temperature data of the autoclave are shared into the Static Structure to calculate the equivalent stress and fatigue life of the autoclave tooth under designated working conditions. By comparing the numerical simulation data of the equivalent stress and fatigue life of the autoclave tooth under 12 working conditions, the variation law of the equivalent stress and fatigue life of the autoclave tooth with the different fillet radii is preliminarily obtained. According to the law of the equivalent stress and fatigue life of the autoclave tooth, the optimization parameter of Direction Optimization is set in the workbench, and the traversal calculation is carried out. The multiobjective optimization of the minimum stress and the maximum fatigue life of the autoclave tooth is finally achieved. The main conclusions are as follows:

(1) The equivalent stress at the autoclave tooth is related to the fillet radius of the autoclave tooth. The maximum equivalent stress at this position decreases first and then increases with the increase of fillet radius, and there is an optimal fillet radius of the autoclave tooth.

(2) The fatigue life of the autoclave tooth is related to the fillet radius at the autoclave tooth. The fatigue life at this position decreases first and then increases with the increase of fillet radius.

(3) The insufficient fatigue life of the autoclave tooth is one of the reasons for the cracks in the root of the autoclave tooth.

(4) The equivalent stress and fatigue life of the autoclave tooth are the same as the optimal fillet radius obtained through the optimization design. The optimal global solution can be obtained through the optimization design process.

Through the numerical simulation of the autoclave tooth, the analysis of the equivalent stress and the fatigue life, and the relationship between the auto-optimization of the fillet radius, will help the autoclave in practical production and optimal design problems of the autoclave.

Data Availability

The data supporting the current study are available from the corresponding author upon request.

Conflicts of Interest

The authors declare that they have no conflicts of interest.

Authors' Contributions

Ouyang Xiaoping conceptualized the study; Lin Pengcheng prepared methodology; Ye Zhijian collected software; Ye Zhijian did validation; Ye Zhijian did formal analysis; Li Yanping did investigation; Ouyang Xiaoping collected resources; Lin Pengcheng contributed data curation; Ye Zhijian wrote the article and prepared the original draft; Ouyang Xiaoping wrote the article and reviewed and edited the article; Li Yanping did visualization; Li Yanping did supervision; Lin Pengcheng administrated the project; Ouyang Xiaoping did funding acquisition. All authors have read and agreed to the published version of the manuscript.

Acknowledgments

The authors thank Dr. Xu Shunyuan for technical assistance. This research was funded by the Huizhou Science and Technology Project, grant number 2021WC010304.

References

[1] C. Chen, H. Sun, Q. Wen, and K. Song, "Design and experimental study of ACFM detection system of autoclave teeth cracks," *Pressure Vessel Technology*, vol. 37, pp. 23–28, 2020.

[2] H. Liu, J. Qin, B. Zhou et al., "Effects of curing pressure on the long-term strength retrogression of oil well cement cured under 200 °C," *Energies*, vol. 15, no. 16, p. 6071, 2022.

[3] B. Backiel-Brzozowska, V. I. Nikitsin, A. Alsabry, S. K. Nikitsin, and W. Rutkowska, "Peculiarities of calculating the thermal conductivity of moist autoclaved aerated concrete," *Energies*, vol. 15, no. 16, p. 5831, 2022.

[4] N. Deliiski, L. Dzurenda, D. Angelski, and N. Tumbarkova, "Influence of selected factors on the duration and energy efficiency of autoclave steaming regimes of non-frozen prisms for veneer production," *Energies*, vol. 14, no. 21, p. 7433, 2021.

[5] A. Kirschner, S. David, G. Brunello et al., "Impact of steam autoclaving on the mechanical properties of 3D-printed resins used for insertion guides in orthodontics and implant dentistry," *Applied Sciences*, vol. 12, p. 6195, 2022.

[6] S. Mollaei, R. Babaei Ghazijahani, E. Noroozinejad Farsangi, and D. Jahani, "Investigation of behavior of masonry walls constructed with autoclaved aerated concrete blocks under blast loading," *Applied Sciences*, vol. 12, no. 17, p. 8725, 2022.

[7] S. A. Stel Makh, E. M. Shcherban, A. N. Beskopylny et al., "Influence of recipe factors on the structure and properties of non-autoclaved aerated concrete of increased strength," *Applied Sciences*, vol. 12, no. 14, p. 6984, 2022.

[8] H. Huang, L. Lu, Y. Huang, and Sun, "JianYe. The test research for flange tooth crack in still kettle body," *Technological Development of Enterprise*, vol. 32, pp. 54-55, 2013.

[9] Z. J. Zhang and L. C. Cao, "Corrosion research of aero-concrete steam autoclave," in *Proceedings of the 9th Vacuum Metallurgy and Surface Engineering Conference*, pp. 175–180, China, August 2009.

[10] Q. Shi, W. Su, and Y. Sun, "Failure analysis and redesign of a poly-condensation autoclave with jacket," *Engineering Failure Analysis*, vol. 97, pp. 480–492, 2019.

[11] H. I. Joshi and G. D. Acharya, "Numerical investigation of design parameters influence on stress distributions in horizontal multi-saddle cylindrical pressure vessel," *Materials Today: Proceedings*, vol. 5, no. 9, pp. 19480–19489, 2018.

[12] Z. Du, H. Li, and Y. Fu, "etc. Steady-state temperature field and stress field analysis of autoclave tooth-locked quick opening structure," *Journal of Mechanical Strength*, vol. 39, pp. 1181–1186, 2017.

[13] H. Li, G. X. Wang, and E. A. Evans, "Numerical analysis of three-dimensional flow in an industry-size hydrothermal autoclave subjected to non-uniform heating," in *Proceedings of the American Society of Mechanical Engineers*, pp. 963–970, Montreal, Quebec, Canada, July 2002.

[14] T. Bohne, T. Frerich, J. Jendrny, J. P. Jürgens, and V. Ploshikhin, "Simulation and validation of air flow and heat transfer in an autoclave process for definition of thermal boundary conditions during curing of composite parts," *Journal of Composite Materials*, vol. 52, no. 12, pp. 1677–1687, 2018.

[15] J. Zhu, T. Frerich, A. Dimassi, M. Koerdt, and A. S. Herrmann, "Experimental validation of a quasi-transient coupling approach for the modeling of heat transfer in autoclave processing," *Journal of Composite Materials*, vol. 56, no. 5, pp. 797–810, 2022.

[16] W. L. Lau, J. Reizes, V. Timchenko, S. Kara, and B. Kornfeld, "Heat and mass transfer model to predict the operational performance of a steam sterilisation autoclave including products," *International Journal of Heat and Mass Transfer*, vol. 90, pp. 800–811, 2015.

[17] Y. Sun, D. Gao, Z. Zhang et al., "Research on air-flow-field characteristics and structural optimization of the guide channels of the autoclave," *Energies*, vol. 15, no. 3, p. 1119, 2022.

[18] N. Kluge, T. Lundström, A.-L. Ljung, L. Westerberg, and T. Nyman, "An experimental study of temperature distribution in an autoclave," *Journal of Reinforced Plastics and Composites*, vol. 35, no. 7, pp. 566–578, 2016.

[19] D. Dolkun, H. Wang, H. J. Wang, and Y. L. Ke, "Influence of large framed mold placement in autoclave on heating performance," *Applied Composite Materials*, vol. 27, no. 6, pp. 811–837, 2020.

[20] T. A. Weber, J. C. Arent, L. Munch, M. Duhovic, and J. M. Balvers, "A fast method for the generation of boundary conditions for thermal autoclave simulation," *Composites Part A: Applied Science and Manufacturing*, vol. 88, pp. 216–225, 2016.

[21] G. N. Xie, J. Liu, W. H. Zang, G. Lorenzini, and C. Biserni, "Simulation and improvement of temperature distributions of a framed mould during the autoclave composite curing process," *Journal of Engineering and Thermophysics*, vol. 22, no. 1, pp. 43–61, 2013.

[22] Y. Fu, H. Huang, T. W. Liu, J. Yuan, and J. Guo, "Failure analysis on kettle tooth cracks of large pressure vessel autoclave," *China Special Equipment Safety*, vol. 31, pp. 121–124, 2015.

[23] Z. Wang, H. Xu, K. S. Guan, and L. Zhang, *Chemical Equipment Failure Principle and Case Analysis*, East China University of Science and Technology Press, Shanghai, China, 2010.

[24] J. Li, "Cause analysis and treatment of crack defect of autoclave," *Guangxi Journal of Light Industry*, vol. 8, 2017.

[25] Y. Dong and Kang, "Chunsheng. Analysis of stress and deformation of steam autoclave swinging device," *Pressure Vessel Technology*, vol. 34, pp. 55–61, 2017.

[26] R. Wu, "Structure design of autoclave mouth based on ANSYS," *Mechanical & Electrical Technology*, vol. 33, pp. 127–129, 2010.

[27] R. Lei, "Discussion on the cause of crack in autoclave," *Mechanical & Electrical Technology*, vol. 35, pp. 118–121, 2012.

[28] S. Su, X. Liu, and B. Li, "Optimization of the wall thickness of super large autoclave based on the Pro/E and workbench," *Machinery Design and Manufacture*, vol. 35, pp. 118–121, 2015.

[29] L. Lu, L. Kong, and W. Chen, "The autoclave inspection and crack analysis," *Chemical Engineering and Equipment*, vol. 585, pp. 75-76, 2014.

[30] J. Chen, "Common defects and cause analysis of autoclave," *Equipment Manufacturing Technology*, vol. 3, 2012.

[31] A. Grbovic and B. Rasuo, "FEM based fatigue crack growth predictions for spar of light aircraft under variable amplitude loading," *Engineering Failure Analysis*, vol. 26, pp. 50–64, 2012.

[32] D. Petrašinović, B. Rašuo, and N. Petrašinović, "Extended finite element method (XFEM) applied to aircraft duralumin spar fatigue life estimation," *Tehnički Vjesnik*, vol. 19, no. 3, pp. 557–562, 2012.

[33] A. Grbović and B. Rašuo, "Use of modern numerical methods for fatigue life predictions," *Recent Trends in Fatigue Design*, vol. 31, 73 pages, 2014.

[34] G. Kastratović, N. Vidanović, A. Grbović, and B. Rašuo, "Approximate determination of stress intensity factor for multiple surface cracks," *FME Transactions*, vol. 46, no. 1, pp. 39–45, 2018.

[35] X. Gu, B. Zhang, Z. Tang, H. Zhang, and H. Wang, "Structural optimization of combine harvester plate–shell undergoing multi-source excitation," *Applied Sciences*, vol. 12, p. 5930, 2022.

[36] R. Xiao, Z. Wang, N. Guo, Y. Wu, J. Shen, and Z. Chen, "Multi-objective motion control optimization for the bridge crane system," *Applied Sciences*, vol. 8, no. 3, p. 473, 2018.

[37] A. Maffezzoli and A. Grieco, "Optimization of parts placement in autoclave processing of composites," *Applied Composite Materials*, vol. 20, no. 3, pp. 233–248, 2013.

[38] T. A. Weber, J. C. Arent, L. Steffens, J. M. Balvers, and M. Duhovic, "Thermal optimization of composite autoclave molds using the shift factor approach for boundary condition estimation," *Journal of Composite Materials*, vol. 51, no. 12, pp. 1753–1767, 2017.

[39] H. Wang, L. Chen, F. Ye, and J. Wang, "A multi-hierarchical successive optimization method for reduction of spring-back in autoclave forming," *Composite Structures*, vol. 188, pp. 143–158, 2018.

[40] M. Dios, P. Gonzalez-R, D. Dios, and A. Maffezzoli, "A mathematical modeling approach to optimize composite parts placement in autoclave," *International Transactions in Operational Research*, vol. 24, no. 1-2, pp. 115–141, 2017.